Soft Matter

Effect of Heterogeneous Network on Glass Transition Dynamics and Solvent Crack Behavior of Epoxy Resins

Journal:	*Soft Matter*
Manuscript ID	SM-ART-04-2020-000625.R1
Article Type:	Paper
Date Submitted by the Author:	06-Jul-2020
Complete List of Authors:	Aoki, Mika; Kyushu University, Center for Polymer Interface and Molecular Adhesion Science Shundo, Atsuomi; Kyushu University, Applied Chemistry Yamamoto, Satoru; Kyushu University, Center for Polymer Interface and Molecular Adhesion Science Tanaka, Keiji; Kyushu University, Department of Applied Chemistry

ARTICLE

Effect of Heterogeneous Network on Glass Transition Dynamics and Solvent Crack Behavior of Epoxy Resins†

Mika Aoki,[a] Atsuomi Shundo,[b,c,d,*] Satoru Yamamoto,[a] and Keiji Tanaka[a,b,c,d,*]

Received 00th January 20xx,
Accepted 00th January 20xx

DOI: 10.1039/x0xx00000x

In general, it has been widely accepted that the physical properties of an epoxy resin are strongly dependent on how it is prepared. However, a clear understanding of the mechanisms of the relationship at a molecular level has yet to be achieved. We here studied the glass transition dynamics and fracture behavior of four epoxy resins, which were pre-cured at different temperatures and well cured under the same conditions. Fourier-transform infrared spectroscopy revealed that the reaction kinetics for an epoxy-amine mixture were strongly dependent on the pre-curing temperature. The glass transition temperature of epoxy resins with the same cross-linking density was dependent on the pre-curing temperature. Dielectric relaxation spectroscopy and dynamic mechanical analysis revealed that the fragility index of the epoxy resin decreased with increasing pre-curing temperature, indicating that the network structure formed in it became more heterogeneous with increasing pre-curing temperature. Once the epoxy resin was immersed in a good solvent, it was partly swollen and was then macroscopically fractured. The fracture was initiated by the crack generation in an un-swollen region of the resin due to the stress induced upon swelling. The immersion time required to reach the fracture decreased as the extent of the heterogeneity increased. The knowledge here obtained should be useful for understanding and controlling fracture toughness of epoxy resins, leading to the furtherance of their functionalization.

1. Introduction

Epoxy resins are an important class of thermosetting resins, which are generally obtained by chemical reactions between epoxy and amino compounds. The reactions lead to the formation of a three-dimensional network expanded over the entire system, resulting in a vitrification, which is accompanied by a freezing of the segmental mobility in between cross-linking points.[1–3] Thus, epoxy resins can be regarded as glassy materials with a network structure that exhibit good corrosion resistance, electronic insulation and mechanical properties.[4–6] These features make epoxy resins promising candidates for a wide range of applications including adhesives,[7–10] coating agents,[11,12] encapsulants,[13–15] composites[16–18] and others. However, epoxy resins are generally brittle and this feature is one of their greatest drawbacks for use as a structural material. A great deal of effort has hitherto been devoted to overcoming this problem. The first step for such would seem to be to examine the relationship between the network structure and fracture toughness.[19–21] Since the network in epoxy resins is often trapped in a glassy state at room temperature, the glassy properties should be taken into account.

The fracture toughness for polymer glasses without any chemical cross-linking has been widely studied.[22–26] Consequently, it is accepted that the toughness of the polymer glasses is related to the molecular weight, or the apparent entanglement density, of the chains.[22,26] This is explained in terms of the deformation and/or craze formation involving the slippage of segments with others.[23,25] Hence, once chemical cross-linking points are introduced into polymer chains, which form the network structure, the chain slippage is expected to be suppressed, leading to an increase in toughness. This should be the case for epoxy resins but is not necessarily so. For example, it has been shown that as the cross-linking density increased, the toughness increased to a maximum and then began to decrease.[27,28] Thus, we are still far from a full understanding of how the frozen network affects the fracture behavior of epoxy resins.

It was recently pointed out that there existed a heterogeneous structure composed of denser and less-dense cross-linked regions in an epoxy resin.[29,30] We also found that the heterogeneous structure generated even at the initial stage of the curing process and the characteristic length scale was dependent on the curing time.[31] Such a heterogeneity in the epoxy resin involving the network structure should play a crucial role in the fracture behavior. In fact, it has been reported that the toughness of epoxy resins was dependent on the curing condition, which altered how the network was formed.[32,33] Nevertheless, there are few studies available on the relationship between the network heterogeneity and fracture toughness of epoxy resins.

In this study, we report on how the network heterogeneity affects the fracture behavior of epoxy resins. To do so, four types of epoxy resins were obtained under different curing conditions, which would generate different extents of heterogeneity. The fragility, which reflects a transient spatial fluctuation in the segmental dynamics near

[a] Center for Polymer Interface and Molecular Adhesion Science, Kyushu University, Fukuoka 819-0395, Japan.
[b] Department of Automotive Science, Kyushu University, Fukuoka 819-0395, Japan.
[c] Department of Applied Chemistry, Kyushu University, Fukuoka 819-0395, Japan.
E-mail: k-tanaka@cstf.kyushu-u.ac.jp, a-shundo@cstf.kyushu-u.ac.jp
[d] International Institute for Carbon-Neutral Energy Research (WPI-I2CNER), Kyushu University, Fukuoka 819-0395, Japan.
† Electronic Supplementary Information (ESI) available: experimental data on Fourier-transform infrared spectroscopy, differential scanning calorimetry, solvent swelling test. See DOI: 10.1039/x0xx00000x

the glass transition, namely dynamic heterogeneity,[34–36] was examined by dielectric relaxation spectroscopy (DRS) in conjunction with dynamic mechanical analysis (DMA). To gain access to the information on the fracture behavior, we here focused on a solvent stress crack method because it needs only a small piece of the specimen. It is also known that once a glassy material contacts in a good solvent, or vapor, the macroscopic fracture occurs due to the development of internal stress.[37] Since epoxy resins are often used in contact with a solvent, the suppression of the solvent stress crack is greatly needed for various applications including structural materials.[38] The knowledge gained from this study would be useful for the design of epoxy resins with better solvent crack resistance.

2. Experimental

2.1. Materials

Panels (a) and (b) of Fig. 1 show the chemical structures of hydrogenated bisphenol-A diglycidyl ether (HDGEBA) and 1,4-cyclohexanebis(methylamine) (CBMA), respectively, purchased from New Japan Chemical Co., Ltd. and Tokyo Chemical Industry Co. For the solvent crack test, tetrahydrofuran (THF) purchased from FUJIFILM Wako Pure Chemical Co. was used as received.

2.2. Preparation of epoxy resins

HDGEBA and CBMA were mixed at a molar ratio of 2:1 at 296 K to initiate the reaction. The mixture was cured via three steps. The first step, named pre-curing, was performed at 283 K for 72 h, 296 K for 24 h, 323 K for 12 h or 353 K for 3 h for four independent mixtures. The second step, named middle-curing, was performed after pre-curing. All samples were middle-cured at 373 K for 1 h, reaching an apparent-completion of the reactions. In the third step, further curing, named post-curing, was conducted at 393 K for 2, 3, 6, 12, 24, 48 and 72 h after the middle-curing. For the DRS and DMA measurements as well as the solvent stress crack test, epoxy resins pre-cured at 283, 296, 323 and 353 K were middle-cured at 373 K, and then post-cured at 393 K for 12, 6, 3 and 2 h, respectively. The discrepancy of the post-curing time among the four epoxy resins was for unifying their cross-linking density. The resins obtained after the three steps are hereafter denoted as ER283, ER296, ER323 and ER353, where the latter number simply corresponds to the pre-curing temperature.

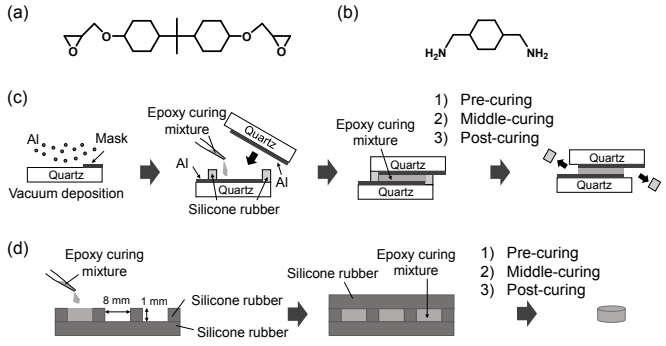

Fig. 1 Chemical structures of (a) HDGEBA and (b) CBMA. Schematic illustrations of sample preparation for (c) DRS measurement and (d) solvent stress crack test.

2.3. Fourier-transform infrared spectroscopy

The curing reaction for the HDGEBA–CBMA mixture was monitored using Fourier-transform infrared (FT-IR) spectroscopy. The mixture was sandwiched between calcium fluoride windows with a 1 mm gap. FT-IR spectra were recorded using a FT/IR-620 spectrometer (JASCO Co.) with a triglycine sulfate (TGS) detector. Measurements were carried out at 283, 296, 323 and 353 K as a function of curing time, until 72, 24, 8 and 3 h, respectively. After these measurements, the samples were middle-cured at 373 K for 1 h and then FT-IR spectra were measured at 296 K. All spectra were obtained with a resolution of 2 cm^{-1} and 64 scans.

2.4. Differential scanning calorimetry

The glass transition temperatures (T_g) were measured by differential scanning calorimetry (DSC) (DSC6220, SII Nanotechnology Inc.). The samples were heated up to 473 K at a rate of 10 $K \cdot min^{-1}$ under a dry nitrogen purge and then cooled down to 273 K. The first heating scan was used for the characterization of T_g.

2.5. Swelling test

The cross-linking density (ν) for the cured epoxy resins was examined by a swelling test. Epoxy resins with a weight (W_0) were immersed in THF at 298 K to reach an equilibrium swelling. The equilibrium weight (W_{eq}) was recorded after collecting fracture pieces and then gently removing THF from the sample surface with blotting paper. The ν value of epoxy resins was calculated on the basis of the Flory-Rehner equation.[39] The mass density of epoxy resins, which was a parameter required for the ν calculation, was examined by a gas pycnometer (ULTRAPYC 1200e, Quantachrome Instruments Inc.).

2.6. Dielectric relaxation spectroscopy

Fig. 1 (c) shows a schematic illustration of the preparation of a parallel-plate capacitor for the DRS measurements. A 100 nm-thick aluminum (Al) layer deposited on a quartz substrate using a VPC-410 vacuum deposition system (ULVAC KIKO Inc.) was used as an electrode. HDGEBA and CBMA were mixed at a molar ratio of 2:1 at 296 K. The HDGEBA–CBMA mixture was sandwiched between Al electrodes with a silicone rubber spacer having a thickness of 100 μm to obtain a parallel-plate capacitor. The active area of the Al electrode was 5 × 4 mm^2. The HDGEBA–CBMA mixture was cured in the capacitor according to the same curing condition described in section 2.2. The thickness of epoxy resins was approximately 100 μm. Dielectric relaxation measurements were taken using a frequency response analyzer (Model SI 1260, Solartron Analytical) combined with a dielectric interface (Model 1296, Solartron Analytical), a temperature controller (Model 335, Lake Shore Cryotronics, Inc.) and a cryostat S-LN/SET1 (JECC TORISHA Co., Ltd.). The complex dielectric permittivity (ε^*), $\varepsilon^*=\varepsilon'-i\varepsilon''$, where ε' and ε'' are the real and imaginary parts, respectively, was recorded isothermally at 383–473 K over a frequency range from 10^0 to 10^5 Hz. The samples were left undisturbed at a given measurement temperature for 5 min to equilibrate prior to the DRS measurements. To confirm the reproducibility of the data and average them, three different specimens for each curing condition were examined.

2.7. Dynamic mechanical analysis

Dynamic mechanical analysis, using a Rheovibron DDV-01FP (A&D Co., Ltd.), was also applied to the epoxy resins prepared under the same curing condition described in section 2.2 to study the segmental dynamics. Sinusoidal strain within the linear response regime was imposed on a sample with a thickness of 300 μm, a width of 3 mm and a length of 30 mm. The measurements were carried out at a heating rate of 2 K·min^{-1} under a dry nitrogen purge. The measurement frequency varied in the range of 0.1−110 Hz. Three different specimens for each curing condition were examined.

2.8. Solvent stress crack test

Solvent crack resistance of the epoxy resin was examined by observing the appearance of the epoxy resin in a solvent. Fig. 1 (d) shows a schematic illustration of the sample preparation for the solvent crack observation. The HDGEBA–CBMA mixture was placed in a mold made of silicone rubber and then cured according to the same curing condition described in section 2.2. After removal from the mold, the samples with a disk-like shape, whose diameter and thickness were 8 and 1 mm respectively, were immersed in THF at 298 K for 72 h. The fracture behavior of epoxy resins in THF was monitored and recorded with a digital camera (iPhone 6s, Apple Inc.).

3. Results and discussion

3.1. Curing reaction

HDGEBA and CBMA were mixed at a molar ratio of 2:1, which was equivalent in stoichiometry of epoxy and amino groups. A primary amino group in CBMA first reacts with an epoxy group in HDGEBA, producing a secondary amino group. This leads to the linear extension. As the secondary amino group further reacts with an epoxy group in HDGEBA, a tertiary amino group is generated, resulting in the formation of the branching structure. Also, if another epoxy group of the HDGEBA molecule leads to a tertiary amino group whether through a secondary amino group, the cross-linking structure is formed. These reactions occurring during the curing process were monitored by FT-IR spectroscopy.

Two absorption bands were observed at 4,524 and 4,940 cm^{-1} in a spectrum for the mixture of HDGEBA and CBMA (see ESI†).[31,40] The former and latter bands are assignable to the combination of the stretching and bending vibrations for epoxy and primary amino groups, respectively.[41] Absorbance for both bands decreased with an increase in curing time, indicating that primary amino and epoxy groups were consumed by the reactions. The consumption rate of epoxy groups (α) can be calculated on the basis of the change in absorbance for epoxy groups (see ESI†).

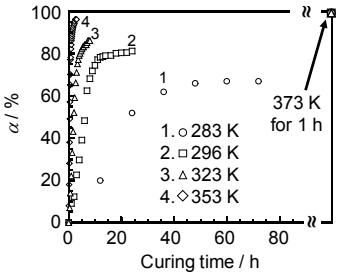

Fig. 2 Curing-time dependence of consumption rate for epoxy groups (α) at 283, 296, 323 and 353 K. The α value after the middle-curing at 373 K for 1 h became nearly 100 %.

Fig. 2 shows the time dependence of the α value for the pre-curing process at 283, 296, 323 and 353 K. The α value increased with increasing time and apparently levelled off after a certain period of time. The rate of increase in α was faster in the order of 353, 323, 296 and 283 K. The curing times, at which α reached a plateau value, were 60, 12, 7 and 2 h for 283, 296, 323 and 353 K, respectively. Also, the plateau αs at 283, 296, 323 and 353 K were 67, 81, 86 and 96 %, respectively. These findings make it clear that the reaction rate became faster as the pre-curing temperature increased. However, it is noteworthy that all α values under the conditions here employed were less than 100 %. This can be explained in terms of the vitrification of the HDGEBA–CBMA mixture during the curing process.[2,31] As the reactions proceed, segments in between cross-linking points become less mobile, meaning that an unreacted epoxy group could not reach into an unreacted amino one and vice-versa. Hence, if the mixture is further heated to promote the mobility of unreacted functional groups, the α value should further increase. This is exactly what was observed after the middle-curing at 373 K which was above the glass transition temperature (T_g), as shown in Fig. 2.

To discuss how the curing temperature affects the network structure including the chain connectivity, the concentration of epoxy groups ([E]) and primary ([A_1]), secondary ([A_2]) and tertiary amino groups ([A_3]) was estimated on the basis of the absorbance change for the bands at 4,524 and 4,940 cm^{-1} (see ESI†). Fig. 3 shows the time-course of concentrations during the pre-curing process at (a) 283, (b) 296, (c) 323 and (d) 353 K. [E] and [A_1] simply decreased with increasing time and their rates became faster with increasing temperature. The time-course of [A_2] was not so simple. While at 283 K, [A_2] increased with time and then leveled off, it maximized at other temperatures. Also, [A_3] simply increased with increasing time

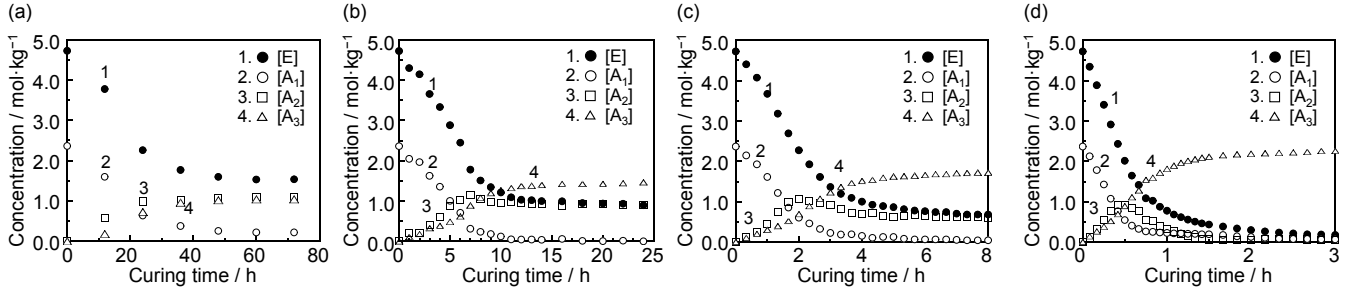

Fig. 3 Curing-time dependence of concentrations for epoxy ([E]) and primary ([A_1]), secondary ([A_2]) and tertiary amino groups ([A_3]) at (a) 283, (b) 296, (c) 323 K and (d) 353 K.

and the rate became faster with increasing temperature. Here, it should be noted that [A_3] almost concurrently increased as [A_2] at 353 K, whereas [A_3] started to increase after [A_2] at other temperatures. Postulating that secondary and tertiary amino groups reflect the linear and branching, or cross-linking, architectures, respectively, it is most likely that the formation process of the network structure was dependent on the pre-curing temperature. This is discussed in more detail in section 3.3.

3.2. Glass transition temperature and cross-linking density

The thermal molecular motion for the post-cured epoxy resins was studied by DSC. For all measurements, the data obtained upon the first heating process were used because once the temperature went beyond T_g, the reactions could further proceed. The T_g value, which was defined as a midpoint of the baseline shift on the DSC chart, increased with post-curing time (t_p) at 393 K and approached a constant value, as shown in Fig. S2 (see ESI†). Taking into account that the α value of epoxy resins middle-cured at 373 K for 1 h was approximately 100 % regardless of the pre-curing temperature, as shown in Fig. 2, the DSC results imply that a tiny amount of unreacted functional groups, which could not be detected by FT-IR, kept reacting with one another upon the post-curing at 393 K until they were completely consumed. In other words, although the α value obtained by FT-IR is a useful indicator of to what extent the reactions proceed, it should be read carefully, especially for a larger α value.

To address to what extent the curing reactions in the middle-cured resins proceeded upon the post-curing process at 393 K, the cross-linking density (ν) in it was examined by the swelling test with THF which is a good solvent for HDGEBA and CBMA as well as epoxy resins. The ν value can be estimated by using the Flory-Rehner equation;[39,42]

$$\nu = \frac{\ln(1-\phi_2)+\phi_2+\chi\phi_2}{V_1\left(\frac{\phi_2}{2}-\phi_2^{\frac{1}{3}}\right)} \quad (1)$$

where, V_1 is the molar volume of THF, and χ is the Flory-Huggins interaction parameter for the epoxy resin with THF, ϕ_2 is the volume fraction of the epoxy resin. Assuming that the χ value is larger than 0.5, χ can be written as[42]

$$\chi \approx \frac{1}{2}+\frac{\phi_2}{3} \quad (2)$$

Here, ϕ_2 is given by

$$\phi_2 = \left[1+\left(\frac{W_{eq}-W_0}{W_0}\right)\left(\frac{\rho_2}{\rho_1}\right)\right]^{-1} \quad (3)$$

W_0 and W_{eq} are the weight of the epoxy resin before and after the swelling. And, ρ_1 and ρ_2 are the mass density of THF and the epoxy resin. The V_1 value can be calculated to be 81.1 $cm^3 \cdot mol^{-1}$ using the molar mass of THF and ρ_1 of 0.889 $g \cdot cm^{-3}$.[43] The ρ_2 value was experimentally obtained as 1.10 $g \cdot cm^{-3}$. For all middle-cured epoxy resins after the 283, 296, 323 and 353 K pre-curing, the relationship between t_p and ν showed a similar trend with the $t_p - T_g$ relationship. That is, the ν value increased with increasing t_p and then reached a constant (see ESI†). This made it possible to correlate ν and T_g.

Fig. 4 shows the relationship between ν and T_g for the post-cured epoxy resins after middle-curing with the 283, 296, 323 and 353 K pre-curing. Regardless of the pre-curing temperature, the T_g value was almost linearly proportional to ν. This can be reasonably understood if we assume that at a higher cross-linking density, the segmental motion of the chains in between the cross-linking points is more effectively suppressed. Here, it is noteworthy that the slope for the ν–T_g relation differs depending on the pre-curing temperature. Consequently, the T_g values of ER283, ER296, ER323 and ER353 were 376, 373, 370 and 366 K, respectively. As stated in the experimental part, they were prepared by the 283, 296, 323 and 353 K pre-curing and followed by the middle-curing at 373 K for 1 h. Then, they were post-cured at 393 K for 12, 6, 3 and 2 h, respectively, so that the cross-linking density in the four epoxy resins became equal. Thus, it is obvious that the pre-curing temperature affects the chain mobility in the resultant resins even after the post-curing. This implies that the network structure developed in the post-cured resins is not independent of the initial one formed during the pre-curing process. Then, the segmental dynamics in the post-cured epoxy resins were studied using DRS in conjunction with DMA.

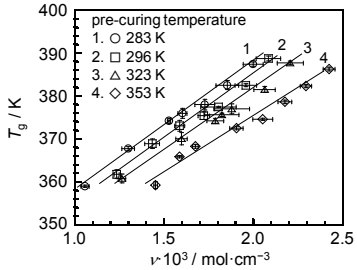

Fig. 4 Relationship between the cross-linking density (ν) and glass transition temperature (T_g) for the post-cured epoxy resins after middle-curing with the 283, 296, 323 and 353 K pre-curing. Solid lines are guides to the eye.

3.3. Segmental dynamics and dynamic heterogeneity

The epoxy resins obtained via different curing processes, ER283, ER296, ER323 and ER353 were characterized by DRS with varying frequency and temperature, which were in the range of 10^0–10^5 Hz and 383–473 K, respectively. Fig. 5 shows frequency dependence of (a) real and (b) imaginary parts of dielectric permittivity (ε' and ε'') for ER296, as a representative example, at 404, 425 and 449 K. Both ε' and ε'' increased with decreasing frequency, especially at a high temperature due to ionic conduction.[44–46]

Since the effect of ionic conduction was superimposed on dielectric functions and thus the molecular dynamics can be difficult to discuss from Fig. 5, complex electric modulus (M^*), which is defined as the inverse quantity of complex permittivity (ε^*) by the

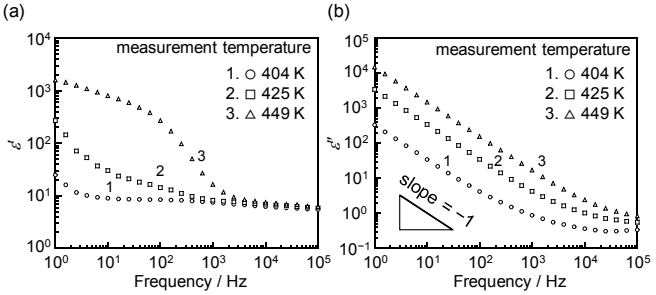

Fig. 5 Frequency dependence of (a) dielectric constant (ε') and (b) dielectric loss (ε'') for ER296.

following equation,[44–46] is here adopted.

$$M^* = \frac{1}{\varepsilon^*} = \frac{\varepsilon'}{\varepsilon'^2 + \varepsilon''^2} + i\frac{\varepsilon''}{\varepsilon'^2 + \varepsilon''^2} = M' + iM'' \quad (4)$$

where M' and M'' are real and imaginary parts of the complex electric modulus, respectively. Examining how M' and M'' depend on the frequency and/or temperature, the molecular motion in an epoxy resin can be discussed.[46] Fig. 6 shows the frequency dependence of (a) M' and M'' for ER296 at 404, 425 and 449 K. An M'' peak was observed accompanied by a distinct change in M' in the frequency range employed. Since the peak frequency shifted to the higher frequency side with increasing temperature, it is apparent that the M'' peak was related to a relaxation process. The M'' peak was fitted by the Havriliak−Negami (HN) function to estimate the relaxation time (τ^{DRS}) for the molecular motion. The NH function is given as follows;[47,48]

$$M'' = M_\infty M_s \times \frac{\left[\left(M_\infty - M_s\right)\sin\gamma\phi\right]A^\gamma}{M_s{}^2A^{2\gamma} + 2A^\gamma\left(M_\infty - M_s\right)M_s\cos\gamma\phi + \left(M_\infty - M_s\right)^2} \quad (5)$$

where

$$M_s = \frac{1}{\varepsilon_s}, \quad M_\infty = \frac{1}{\varepsilon_\infty} \quad (6)$$

$$A = \left[1 + 2\left(\omega\tau_{HN}\right)^{1-\alpha_D}\sin\frac{\alpha_D\pi}{2} + \left(\omega\tau_{HN}\right)^{2(1-\alpha_D)}\right]^{\frac{1}{2}} \quad (7)$$

$$\phi = \text{atan}\left[\frac{\left(\omega\tau_{HN}\right)^{1-\alpha_D}\cos\frac{\alpha_D\pi}{2}}{1 + \left(\omega\tau_{HN}\right)^{1-\alpha_D}\sin\frac{\alpha_D\pi}{2}}\right] \quad (8)$$

$$\tau^{DRS} = \tau_{HN}\left[\frac{\sin\pi\alpha_D\gamma}{\frac{2+2\gamma}{\sin\pi\alpha_D}}\right]^{\frac{1}{\alpha_D}} \quad (9)$$

and, ε_s and ε_∞ are the dielectric constants for the low- and high-frequency sides of relaxation, respectively, α_D and γ are the parameters describing the asymmetric and symmetric broadening.

Fig. 7(a) shows a semi-logarithmic plot of τ^{DRS} against the inverse temperature (T^{-1}) for ER283, ER296, ER323 and ER353. To compare directly the data set among the four epoxy resins, the abscissa of Fig. 7 is normalized using each T_g value, provided as the Angell plot.[35] The temperature dependence of τ^{DRS} for all epoxy resins exhibited non-Arrhenius behavior and could be well expressed by the Vogel-Fulcher-Tamman (VFT) equation;[49–51]

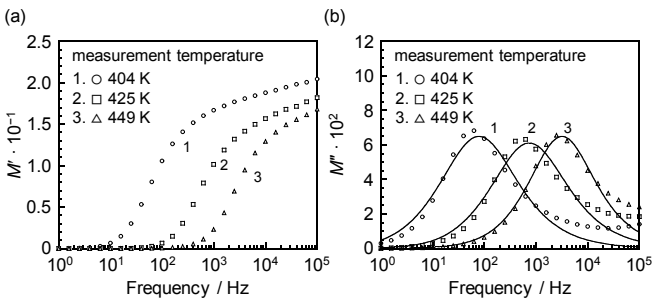

Fig. 6 Frequency dependence of (a) real and (b) imaginary parts of electric modulus (M' and M'') for ER296. Solid symbols denote experimental data and solid lines are the best fit curves based on the HN equation.

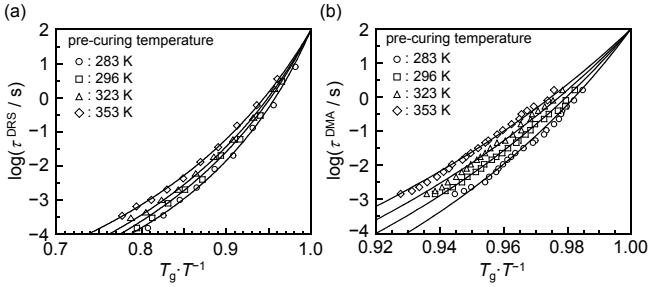

Fig. 7 Semi-logarithmic plots of relaxation time against inverse of temperature for ER283, ER296, ER323 and ER353 obtained by (a) DRS and (b) DMA. The temperature is normalized by T_g. Open symbols denote experimental data and solid curves are the best-fit based on the VFT equation.

$$\tau = \tau_0 \cdot \exp\left(\frac{B}{T - T_0}\right) \quad (10)$$

where B is the activation temperature, T_0 is the Vogel temperature and τ_0 is the relaxation time at a high temperature limit. Solid curves in Fig. 7 denote the best fit by the VFT equation using fitting parameters of B, T_0 and τ_0. Table 1 summarizes fitting parameters together with the dynamic T_g value (T_g^{DRS}), which is calculated as the relaxation temperature at τ^{DRS} = 100 s.[52] The T_g^{DRS} values for the four resins were in good accordance with the T_g values by DSC. The fragility index (m) was estimated using the following equation;[35]

$$m = \left.\frac{d\log(\tau)}{d\left(T_g/T\right)}\right|_{T=T_g} \quad (11)$$

The fragility corresponds to an apparent activation energy for the α-relaxation process at near the glass transition. Glass forming systems with larger and smaller m values are referred to as fragile and strong, respectively.[35] As a result, the values of the fragility index (m^{DRS}) for ER283, ER296, ER323 and ER353 were 56 ± 1, 50 ± 1, 47 ± 1 and 45 ± 2, respectively.

DRS has an advantage over DMA that the frequency range of the measurement was broader. However, the origin of the relaxation process discussed in the above based on M'' is not straightforward to understand due to the contribution from the direct current component. Since the temperature dependence of τ^{DRS} can be well expressed by the VFT equation, there is no doubt that the relaxation process is somehow correlated to the segmental motion. Hence, the DMA measurements, which enable us to gain direct access to the segmental dynamics, were conducted. The temperature dependence of storage (E') and loss moduli (E'') for ER296, as a representative example, at various frequencies ranging from 0.1 to 110 Hz was shown in Fig. S6 (see ESI†). Fig. 7 (b) shows the Angell plot for ER283, ER296, ER323 and ER353. The data were again fitted by the VFT equation.

Table 1 Fitting parameters with the dynamic T_g value estimated from the DRS data (T_g^{DRS}), which is the relaxation temperature at τ^{DRS} = 100 s, and fragility index (m^{DRS}) for ER283, ER296, ER323 and ER353.

sample	B	T_0 / K	T_g^{DRS} / K	T_g / K	m
ER283	1506 ± 20	313 ± 1	380 ± 0.3	376 ± 1	56 ± 1
ER296	1839 ± 21	296 ± 1	374 ± 0.4	373 ± 1	50 ± 1
ER323	1893 ± 38	290 ± 1	371 ± 1	370 ± 1	47 ± 1
ER353	1868 ± 53	285 ± 2	367 ± 1	366 ± 0.3	45 ± 2

Table 2 Fitting parameters with the dynamic T_g value (T_g^{DMA}) and fragility index (m^{DMA}) for ER283, ER296, ER323 and ER353.

sample	B	T_0 / K	T_g^{DMA} / K	T_g / K	m^{DMA}
ER283	1703 ± 37	330 ± 2	376 ± 1	376 ± 1	130 ± 3
ER296	1997 ± 45	319 ± 1	374 ± 1	373 ± 1	110 ± 2
ER323	2200 ± 82	310 ± 1	370 ± 1	370 ± 1	99 ± 3
ER353	2533 ± 47	298 ± 2	366 ± 1	366 ± 0.3	85 ± 3

Table 2 summarizes the results containing the dynamic T_g (T_g^{DMA}) and the fragility index (m^{DMA}). Although the values of m^{DRS} and m^{DMA} were not the same as each other, it is obvious that the fragility index was lower in the order of ER353, ER323, ER296 and ER283. The difference between the m^{DRS} and m^{DMA} values can be explained by what is observed by the DRS and DMA measurements; the former basically detects the motion of charge carrier coupled with the segmental motion while the latter does the segmental motion itself.

According to a previous report based on the incoherent elastic scattering technique using neutrons,[53] the magnitude of the m value has been discussed in terms of dynamic heterogeneity, which is a transient spatial fluctuation in the segmental dynamics near the glass transition. A lower m suggests a greater extent of the dynamic heterogeneity in the system.[53] Postulating that the discussion works for the current study, the extent of the dynamic heterogeneity is supposed to be greater in the order of ER353, ER323, ER296 and ER283. This order is the same as for the temperature of the pre-curing for epoxy resins.

To discuss the difference of the m value among the four samples, it is first considered how the pre-curing temperature affects the formation of the network structure. As revealed by FT-IR spectroscopy, the formation manner of the network was dependent on the pre-curing temperature. In short, while secondary amines were initially generated and then converted to tertiary amines at a lower temperature, the initial stage involved the generation both of secondary and tertiary amines at a higher temperature. Such a conversion behavior was previously observed and two different types of formation of the epoxy-amine network were proposed to explain it.[29]

Fig. 8 shows a schematic illustration for the two modes of the network formation process. In panel (a), linear chains initially grew until the formation of a low-density network expanded over the system, a so-called skeleton network, and then unreacted species cross-linked the inside of the skeleton network. Panel (b) shows the initial growth of the cross-linked domains, or microgels, followed by their interconnection. The former and latter types are expected to produce relatively homogeneous and heterogeneous networks, respectively.[29,31] Thus, it is plausible that a higher pre-curing temperature provides a more heterogeneous network, in which denser and less dense regions exist. Given that the network formed by pre-curing is somehow preserved even after middle-curing and post-curing, the extent of the network heterogeneity should be greater in the order of ER353, ER323, ER296, ER283.

The T_g value is generally related to the cross-linking density of the network, ν.[54] On the other hand, the T_g value was here lower in the order of ER353, ER323, ER296 and ER283 which each possessed an identical ν. The difference between the four resins was the heterogeneity. Since the heterogeneous network contains dangling chains, in which one end attaches to the network and the other is free,

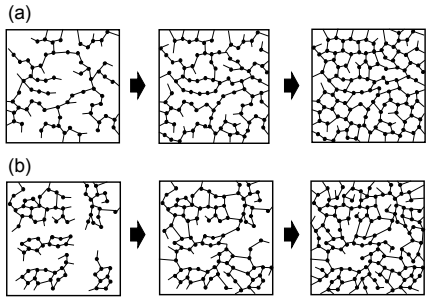

Fig. 8 Schematic illustrations for two different types of network formation expected for the pre-curing at (a) lower and (b) higher temperatures.

the free volume becomes larger with a larger heterogeneity, leading to a lower T_g.[55,56] This may also be explained in terms of the fragility. Taking the heterogeneous network into account, it is expected that the chain mobility in the higher cross-linked and less cross-linked regions is suppressed and not suppressed, respectively. This can be seen as the system starts to vitrify. In the case of glass formers, once the temperature decreases and approaches T_g, the vitrification occurs.[2] At the initial stage of the process, a domain, named a cooperative rearrangement (CRR) region, is formed.[57–59] As the vitrification further proceeds, the domain evolves in size and eventually expands over the entire system by connecting with one another at a temperature below T_g.[60] This picture would explain the heterogeneity in the segmental dynamics near the glass transition, namely the m value. In our current study, the epoxy resin starts to vitrify as the reaction proceeds, resulting in the formation of the higher cross-linked and less cross-linked regions. Thus, the difference in the m value between ER353, ER323, ER296 and ER283 can be associated with the heterogeneous network.

3.4. Macroscopic behavior of solvent stress crack

Finally, the solvent crack behavior for ER283, ER296, ER323 and ER353 was examined. Fig. 9 shows photographs of ER283, ER296, ER323 and ER353, which were immersed in THF after (a) 0, (b) 10, (c) 12, (d) 21 and (e) 31 h. All epoxy resins were partly swollen and then spontaneously disrupted. However, the time at which the macroscopic fracture occurred was dependent on the pre-curing temperature; it was shorter in the order of ER353, ER323, ER296 and ER283. Here, it should be noted that there was no significant difference in the swelling rate among the four samples (see ESI†). Thus, the shorter fracture time indicates that the epoxy resin having a lower m value, namely more heterogeneous in terms of the network structure, was more easily disrupted upon swelling with THF. To discuss why the solvent crack behavior depended on the pre-curing temperature, or heterogeneity, the swelling process of the epoxy resin was optically observed under a cross-polarized condition.

Fig. 10 shows photographs of the representative sample, ER296 in THF, at various immersion times. A cross-shaped dark region observed for all images originated from a geometric feature of a conoscope, a so-called isogyre.[61] The swelling started from the circumference edge of the specimen. The swollen and un-swollen regions co-existed at the early state of the swelling process. An isochromatic striped pattern due to the birefringence was observed in the swelling region and it was along the direction parallel to the

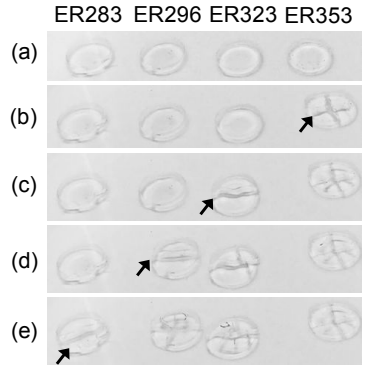

Fig. 9 Photographs of ER283, ER296, ER323 and ER353 immersed in THF after (a) 0, (b) 10, (c) 12, (d) 21 and (e) 31 h. Arrows show macroscopic cracks generated in the specimens.

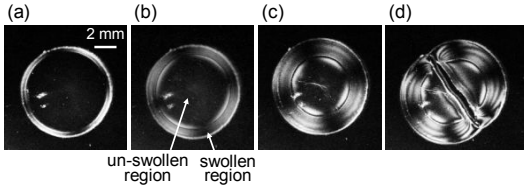

Fig. 10 Photographs of ER296 immersed in THF after (a) 0, (b) 10, (c) 20 and (d) 25 h, which were observed under the crossed-Nicols condition.

circumference edge. In the swelling region, segments in the network are supposed to be elongated and oriented possibly due to the gradient of chemical potential of the segments.[62] In general, an isochromatic striped pattern appears along the direction normal to the stress.[62,63] Thus, the photographs imply that the elongational stress was generated along the direction from the center to the circumference edge of the circular sample upon swelling. After a while, the swollen region was expanded. That is, the elongational stress in the sample increased. Concurrently, a crack appeared in the un-swollen region, most probably from the circular center at which the stress was maximized, leading to the macroscopic fracture. Since the macroscopic fracture occurred by cracking in the un-swollen region, it seems reasonable to consider that the difference in the fracture time among the four epoxy resins, seen in Fig. 10, reflects their bulk fracture toughness.

Previously, it was reported that an epoxy network with a higher cross-linking density attained a denser glassy state after vitrification.[64] Once the heterogeneous network was vitrified, the higher and less cross-linking regions would become dense and less-dense glassy regions, respectively. The less-dense glassy regions in the epoxy resin should be mechanically weak in comparison with the dense glassy regions. In general, the stress imparted upon a deformation process is concentrated on mechanically weak regions, at which cracking occurs and eventually leads to the fracture.[26,65,66] Taking into account that the extent of the network heterogeneity was greater in the order of ER353, ER323, ER296 and ER283, it is reasonable that the fracture time upon swelling is shorter in that order.

4. Conclusions

We studied the physical properties including the glass transition behavior, heterogeneity and solvent crack behavior for epoxy resins obtained via different curing processes. Epoxy resins used in this study were obtained by pre-curing a mixture of HDGEBA and CBMA at four different temperatures, 283 K, 296 K, 323 K and 353 K and followed by middle-curing to reach an apparent completion of the reactions. Then, they were post-cured for various times. DRS and DMA measurements revealed that the *m* value of the epoxy resin decreased with increasing pre-curing temperature, indicating that a transient spatial fluctuation in the segmental dynamics near the glass transition temperature, namely dynamic heterogeneity, became more apparent. Such a smaller *m* can be associated with the heterogeneous network, in which denser and less-dense cross-linked regions exist, formed by the different chemical reactions during the pre-curing, as suggested by FT-IR spectroscopy. The four types of epoxy resins showing different network heterogeneity were examined by a solvent stress crack test in conjunction with the birefringence observation. Once the epoxy resin was immersed in THF, which was a good solvent, the resin was partly swollen and was then macroscopically fractured. The immersion time at which the macroscopic fracture occurred decreased as the extent of the heterogeneity increased. This can be reasonably understood if we consider that the stress is concentrated on the less-dense regions. The knowledge here obtained should be useful for understanding and controlling the fracture toughness of epoxy resins, leading to the furtherance of their functionalization.

Conflicts of interest

There are no conflicts to declare.

Acknowledgements

We would express our deep thanks to Prof. Koji Fukao, Ritsumeikan University, for discussion about DRS measurements. This research was partly supported by JSPS KAKENHI, Grant-in-Aid for Scientific Research (B) (no. JP19H02780) (A.S.) and JST-Mirai Program (JPMJMI18A2) (K.T.).

Notes and references

1. C.-Y. M. Tung and P. J.Dynes, *J. Appl. Polym. Sci.*, 1982, **27**, 569−574.
2. S. Montserrat, *J. Appl. Polym. Sci.*, 1992, **44**, 545−554.
3. S. Corezzi, D. Fioretto, D. Puglia and J. M. Kenny, *Macromolecules*, 2003, **36**, 5271–5278.
4. N. Yousefi, X. Sun, X. Lin, X. Shen, J. Jia, B. Zhang, B. Tang, M. Chan and J.-K. Kim, *Adv. Mater.*, 2014, **26**, 5480–5487.
5. C. He, S. Shi, X. Wu, T. P. Russell and D. Wang, *J. Am. Chem. Soc.*, 2018, **140**, 6793−6796.
6. K. Chen, X. Kuang, V. Li, G. Kang and H. J. Qi, *Soft Matter*, 2018, **14**, 1879–1886.
7. E. Chabert, J.Vial, J.-P. Cauchois, M. Mihalutac and F. Tournilhac, *Soft Matter*, 2016, **12**, 4838–4845.
8. S. Pruksawan, S. Samitsu, H. Yokoyama and M. Naito, *Macromolecules*, 2019, **52**, 2464–2475.
9. R. Mo, J. Hu, H. Huang, X. Sheng and X. Zhang, *J. Mater Chem. A*, 2019, **7**, 3031–3038.
10. Q.-V. Bach, C. M. Vu, H. T. Vu, T. Hoang, T. V. Dieu and D. D. Nguyen, *Polym. J.*, 2020, **52**, 345–357.
11. N. Hameed, N. V. Salim, T. L. Hanley, M. Sona, B. L. Fox and

Q. Guo, *Phys. Chem. Chem. Phys*., 2013, **15**, 11696–11703.
12. Y. Huang, L. Deng, P. Ju, L. Huang, H. Qian, D. Zhang, X. Li, H. A.Terryn and J. M. C. Mol, *ACS Appl. Mater. Interfaces*, 2018, **10**, 23369–23379.
13. S. C. Yang, S.-Y. Kwak, J. H, Jin,a J.-S. Kim, Y. Choi, K.-W. Paik and B.-S. Bae, *J. Mater. Chem*., 2012, **22**, 8874–8880.
14. M. Aoki, A. Shundo, K. Okamoto, T. Ganbe and K. Tanaka, *Polym. J.*, 2019, **51**, 359−363.
15. S. Yamamoto, R. Kuwahara, M. Aoki, A. Shundo and K. Tanaka, *ACS Appl. Polym. Mater.*, 2020, DOI: 10.1021/acs.iecr.9b04652.
16. A. V. Pansare, S. R. Khairkar, A. A. Shedge, S. Y. Chhatre, V. R. Patil and A. A. Nagarkar, *Adv. Mater.*, 2018, **30**, 1801523.
17. R. Aoki, A. Yamaguchi, T. Hashimoto, M. Urushisaki, T. Sakaguchi, K. Kawabe, K. Kondo and H. Iyo, *Polym. J.*, 2019, **51**, 909–920.
18. K. Yang, J. Guan and K. Numata, C. G. Wu, S. J. Wu, Z. Z. Shao, R. O. Ritchie, *Nat. Commun.*, 2019, **10**, 3786.
19. G. Levita, S. De Petris, A. Marchetti and A. Lazzeri, *J. Mater. Sci.*, 1991, **26**, 2348–2352.
20. A. Izumi, T. Nakao and M. Shibayama, *Soft Matter*, 2012, **8**, 5283–5292.
21. R. Rahul and R. Kitey, *Composites Part B Eng.*, 2016, **85**, 336–342.
22. E. Kramer, *J. Mater. Sci.*, 1979, **14**, 1381–1388.
23. A. M. Donald and E. J. Kramer, *J. Polym. Sci., Polym. Phys. Ed.*, 1982, **20**, 899–909.
24. L. Kogan, C.-Y. Hui and A. Ruina, *Macromolecules*, 1996, **11**, 4090–4100.
25. J. Liu and A. F. Yee, *Macromolecules*, 2000, **33**, 1338–1344.
26. A. Sánchez-Valencia, O. Smerdova, L. R. Hutchings and D. S. A. De Focatiis, *Macromolecules*, 2017, **50**, 9507–9514.
27. J. P. Bell, *J. Appl. Polym. Sci.*, 1970, **14**, 1901−1906.
28. K. Cho, D. Lee, C. E. Park and W. Huh, *Polymer*, 1996, **37**, 813−817.
29. C. M. Sahagun and S. E. Morgan, *ACS Appl. Mater. Interfaces*, 2012, **4,** 564–572.
30. S. Morsch, Y. Liu, S. B. Lyon and S. R.Gibbon, *ACS Appl. Mater. Interfaces*, 2016, **8**, 959–966.
31. M. Aoki, A. Shundo, R. Kuwahara, S. Yamamoto and K. Tanaka, *Macromolecules*, 2019, **52**, 2075–2082.
32. S. Mostovoy, E. J. Ripling and C. F. Bersch, *J. Adhes.*, 1971, **3**, 125–144.
33. R. Ramsdale-Capper and J. P. Foreman, *Polymer*, 2018, **146**, 321–330.
34. K. L. Ngai and C. M. Roland, *Macromolecules*, 1993, **26**, 6824–6830.
35. C. A. Angell, *Science*, 1995, **267**, 1924–1935.
36. M. D. Ediger, *Annu. Rev. Phys. Chem.*, 2000, **51**, 99–128.
37. Y.-F. Chuang, H.-C. Wu, F. Yang, T.-J. Yang and S. Lee, *J. Polym. Res.*, 2017, **24**, 2.
38. A. Toscano, G. Pitarresi, M. Scafidi, M. Di Filippo, G. Spadaro and S. Alessi, *Polym. Degrad. Stabil.*, 2016, **133**, 255–263.
39. M. Rubinstein and R. H. Colby, Polymer Physics, Oxford University Press, Canada, 2003.
40. T. Hirai, K. Kawasaki and K. Tanaka, *Phys. Chem. Chem. Phys.*, 2012, **14**, 13532–13534.
41. C. C. Riccardi, H. E. Adabbo and R. J. J. Williams, *J. Appl. Polym. Sci.*, 1984, **29**, 2481–2492.
42. W. Xue, S. Champ and M. B. Huglin, *Polymer*, 2001, **42**, 3665−3669.
43. B. Cartigny, N. Azaroual, M. Imbenotte, N. Sadeg, F. Testart, J. Richecoeur, G. Vermeersch and M. Lhermitte, *J. Anal. Toxicol.*, 2001, **25**, 270–274.
44. W. Jilani, N. Mzabi, N. Fourati, C. Zerrouki, O. Gallot-Lavallée, R. Zerrouki and H. Guermazi, *Polymer*, 2015, **79**, 73–81.
45. P. Zhang, Y. Bin, R. Zhang and M. Matsuo, *Polym. J.*, 2017, **49**, 839–850.
46. W. Jilani, N. Mzabi, N. Fourati, C. Zerrouki, O. Gallot-Lavallée, R. Zerrouki and H. Guermazi, *J. Mater. Sci.*, 2016, **51**, 7874–7886.
47. S. Havriliak and S. Negami, *J. Polym. Sci. C*, 1966, **14**, 99–117.
48. G. M. Tsangaris, G. C. Psarras and N. Kouloumbi, *J. Mater. Sci.*, 1998, **33**, 2027– 2037.
49. H. Vogel, *Phys. Z*, 1921, **22**, 645–646.
50. G. S. Fulcher, *J. Am. Ceram. Soc.*, 1925, **8**, 339–355.
51. G. Tammann and W. Hesse, *Z. Anorg. Allg. Chem.* 1926, **156**, 245–257.
52. T. Hirata, H. Matsuno, D. Kawaguchi, M. Inutsuka, T. Hirai, M. Tanaka and K. Tanaka, *Phys. Chem. Chem. Phys.*, 2017, **19**, 1389–1394.
53. T. Kanaya, I. Tsukushi and K. Kaji, *Prog. Theor. Phys. Suppl.*, 1997, **126**, 133–140.
54. W. D. Cook, M. Mehrabi and G. H. Edward, *Polymer*, 1999, **40**, 1209–1218.
55. C. Feger and W. F. MacKnight, *Macromolecules*, 1985, **18**, 280–284.
56. Q. Xie, S. Liang, B. Liu, K. Fu, Z. Zhan, L. Lu, X. Yang, F. Lü and Z. Huang, *AIP Adv.*, 2018, **8**, 075332.
57. E. Donth, *J. Non-Cryst. Solids*, 1982, **53**, 325−330.
58. E. V. Russell and N. E. Israeloff, *Nature*, 2000, **408**, 695−698.
59. J. D. Stevenson, J. Schmalian and P. G.Wolynes, *Nat. Phys.*, 2006, **2**, 268–274.
60. D. Cangialosi, A. Alegría and J. Colmenero, *Phys. Rev. E*, 2007, **76**, 011514.
61. P. Wang, *Opt. Lett.*, 2012, **37**, 4392–4394.
62. Y. Maki, K. Furusawa, S. Yasuraoka, H. Okamura, N. Hosoya, M. Sunaga, T. Dobashi, Y. Sugimoto and K. Wakabayashi, *Carbohydr. Polym.*, 2014, **108**, 118–126.
63. M. Ramji and K. Ramesh, *Opt. Lasers Eng.*, 2008, **46**, 257–271.
64. Y. Yarovskya and E. Evans, *Polymer*, 2002, **43**, 963–969.
65. S. Yamini and R. J. Young, *J. Mater. Sci.*, 1980, **15**, 1823–1831.
66. Y. Matsumoto, A. Shundo, H. Hayashi, N. Tsuruzoe and K. Tanaka, *Macromolecules*, 2019, **52**, 8266–8274.

Table of Contents

Network structure in an epoxy resin, which became more heterogeneous with increasing pre-curing temperature, affected the glass transition dynamics and solvent crack behavior.